ACS Catalysis

Research Article

pubs.acs.org/acscatalysis

Theoretical Study of a "Surface Explosion": Decomposition of Acetic Acid on Rh Surfaces

Xue-Rong Shi, Daniel Wei, and David Sholl*

School of Chemical & Biomolecular Engineering, Georgia Institute of Technology, 311 Ferst Drive, Atlanta, Georgia 30332-0100, United States

Supporting Information

ABSTRACT: The "surface explosion" associated with decomposition of acetic acid on Rh surfaces is studied by density functional theory. The surface configuration of adsorbed acetate and the reaction paths available to the adsorbed species are determined. The reactivity of adsorbed acetate is found to be dependent on the local surface coverage, which allows a model explaining the experimentally observed surface explosion to be developed. Comparison of the reactivity of different surfaces shows that Rh(111) is more active than the Rh(110) surface for both clean and oxygen precovered surfaces, and the oxygen precovered surfaces are less active than the clean surfaces.

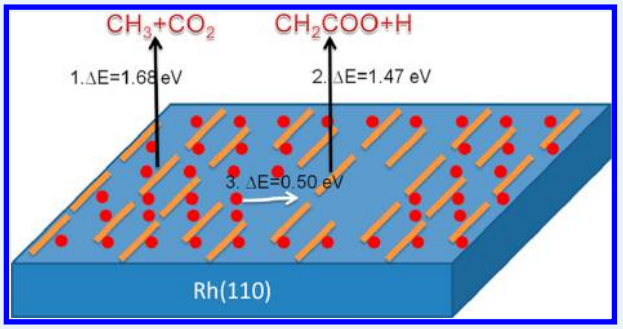

KEYWORDS: *density functional theory (DFT), surface explosion, acetic acid, Rh(111), Rh(110), clean surface, oxygen precovered surface*

1. INTRODUCTION

Molecular desorption during temperature programmed desorption (TPD) typically occurs over a significant span of temperatures. In some situations, however, an autocatalytic process causes adsorbed species to completely desorb within a very narrow temperature range. This situation has been described as a "surface explosion".[1−10] Surface explosions have been reported for, among others, malic acid on Cu(110),[11] tartaric acid on Cu(110),[12−14] acetic acid on Ni(110),[15] and acetic acid coadsorbed with oxygen or carbon on Rh(111), Rh(110), and Pd(110).[16−20] All of these molecules are adsorbed in a deprotonated form, and they decompose into CO_2, H_2O, H_2, and so forth during desorption. Although various phenomenological models for surface explosions have been described,[21−25] we are not aware of any work that provides a molecular-scale description of this phenomenon for any specific material. In this paper, we aim to use density functional theory (DFT) calculations to understand the specific mechanism that causes the surface explosion during decomposition of acetic acid on Rh surfaces.

The decomposition of acetic acid has been experimentally examined for Rh(110), Rh(111), and supported Rh particles.[16,18,19,26,27] When these surfaces are exposed to acetic acid at ∼300 K, the acetic acid decomposes into acetate and releases H_2 into the gas phase. Li et al. found that an essential requirement for a surface explosion is the presence of a coadsorbed atomic species such as O atoms.[26] Oxygen is found to stabilize acetate and causes it to decompose at a higher temperature.[18,26] On the clean Rh(111) surface, TPD yields a peak maximum at 390 K and a peak width of ∼26 K. For an oxygen precovered Rh(111) surface, the peak temperature varies from ∼410 K to ∼500 K and the peak width varies from 7 to 16 K depending on the amount of precovered oxygen.[26] On the clean Rh(110) surface, TPD gives a peak of 391 K with a width of ∼30 K, whereas on oxygen-precovered surfaces, the peak temperature is 465 K with a peak width of 16 K.[18,26] With an oxygen precovered Rh/Al_2O_3 surface, TPD shows two CO_2 desorption peaks due to the decomposition of acetate. The low temperature desorption shoulder exhibits a surface explosion with a full width at half-maximum (fwhm) of ∼8 K, consistent with acetate decomposition on the Rh particles. The high temperature peak is more consistent with acetate decomposition on the Al_2O_3 support.[17] Without predosed oxygen, there is no obvious formation of acetate on the Rh component of this supported catalyst. The presence of acetate on the support is believed to result from the spillover of the acetate from the metal to favored sites on the support, similar to other reports of formate spillover on a Rh/Al_2O_3 catalyst.[28]

Several possible reasons have been proposed to explain the mechanism of the acetate surface explosion on Rh:[16,17] (1) Surface reconstruction induced by preadsorbed oxygen that influences the decomposition kinetics, (2) adsorbate-induced ordering in which dense layers of the adsorbed molecules form a structure that inhibits decomposition and weakens adsorption, and (3) site blocking by the adsorbate in which the coadsorbed adatom blocks sites adjacent to the acetate which are necessary for decomposition. No experimental evidence exists to support the idea of a surface reconstruction

Received: September 17, 2013
Revised: January 31, 2014
Published: February 4, 2014

leading to the observed surface explosions. Specific ordered adlayers have been proposed for acetate on O−Rh(110)[16] and on clean Pd(110), where a surface explosion is also observed,[20] although the experimental support for either of these structures is limited.

In this paper, we present results from theoretical studies on the decomposition of acetic acid on Rh(111) and Rh(110) to shed light on the surface explosions seen on these surfaces. In Section 2, we describe our computational methods. Section 3 present results of calculations that describe adsorption of acetate and reaction paths for decomposition of adsorbed acetate. This allows us to propose a specific mechanism that controls the surface explosions observed on oxygen precovered surfaces. Section 4 compares the reactivity of different surfaces and the role of oxygen and also compares simulated TPD results from a model derived from our DFT calculations and experimental data. By explaining the mechanism controlling this specific instance of a surface explosion, our results should be useful in understanding this phenomenon in other systems.

2. MODELS AND METHODS

All DFT calculations were performed with plane-wave DFT[29] using the Vienna ab initio simulation package (VASP) with the Perdew−Wang generalized gradient exchange-correlation functional and the projector augmented wave (PAW) method.[30−35] Spin polarization was employed for all calculations, and the cutoff energy for the plane wave basis set was fixed at 400 eV. Geometry optimization was performed with a conjugate-gradient algorithm and considered to be converged when the forces on each unconstrained atom was <0.03 eV/Å. A Monkhorst−Pack grid of 3 × 2 × 1 and 4 × 4 × 1 k-points was employed for the Rh(110) and Rh(111) surface, respectively. Transition states (TS) were identified by the climbing-image NEB method and were confirmed by vibrational analysis to have only one imaginary frequency.[36,37]

For the clean and oxygen precovered Rh(110) surface, we employed a 4 × 2 surface unit cell and a slab made up of eight atomic layers. For the clean and oxygen precovered Rh(111) surface, we used a 2 × 2 surface unit cell and a slab three layers thick. All slab calculations used a vacuum spacing of at least 12 Å normal to the surface. Preliminary calculations indicated that these supercells were adequate to give well-converged results.[38]

In experiments with O-covered surfaces, the Rh(110) and Rh(111) surface are exposed to the molecular oxygen to obtain an oxygen-saturated surface. By combining scanning tunneling microscopy, core level spectroscopy, and DFT calculations, a maximum oxygen coverage of 1 ML (where 1 ML corresponds to one adsorbate per surface metal atom) has been described for Rh(110) surface under 300 K.[39] At this coverage, O adatoms occupy 3-fold sites in a zigzag arrangement along $[1\bar{1}0]$ rows, as shown in Figure 1a. The saturated oxygen coverage for the Rh(111) surface was determined to be 0.5 ML.[26] By DFT calculations, it was found that oxygen occupies the fcc hollow site rather than the hcp hollow site, as shown in Figure 1b.[40] We used the models shown in Figure 1 for our subsequent descriptions of oxygen precovered Rh(110) and Rh(111).

Adsorption energies, E_{ads}, were calculated by

$$E_{ads} = E_{total}(ads/surf) - E_{total}(ads) - E_{total}(surf) \quad (1)$$

where the terms on the right-hand side are the total energies of the Rh surface with adsorbates in their equilibrium geometries, the free adsorbates in gas phase, and the clean Rh surface,

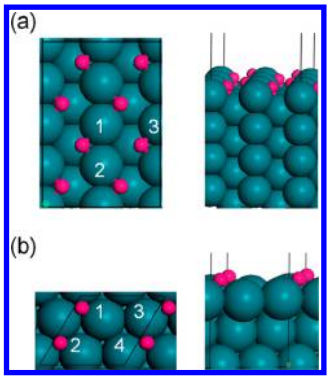

Figure 1. Oxygen precovered Rh surface used in this work: (a) O−Rh(110) and (b) O−Rh(111). Left: top view; right: side view. Small pink spheres: O; large blue spheres: Rh. Surface reaction sites are labeled by numbers. The boxes indicate the computational supercells.

respectively. Reaction energies, ΔE_r, for reactions of the form AB →A + B were calculated by

$$\Delta E_r = E_{total}(A/surf) + E_{total}(B/surf) - E_{total}(AB/surf) - E_{total}(surf) \quad (2)$$

where E_{total} (A/surf), E_{total}(B/surf), and E_{total}(AB/surf) are the total energies for the separately adsorbed A, B, and AB on the Rh surface, respectively. With these definitions, adsorption energies that are more negative correspond to more favorable configurations, and reaction energies that are negative correspond to exothermic reactions. To compare reaction barriers on the oxygen precovered and clean surface, we define $\Delta(\Delta E)$ as

$$\Delta(\Delta E) = \Delta E(O) - \Delta E = [E_{ads-reactant} - E_{ads-reactant}(O)] + [E_{ads-TS}(O) - E_{ads-TS}] \quad (3)$$

where $\Delta E(O)$ and ΔE are the reaction barriers on the oxygen precovered and clean surface, respectively, and ads-reactant and ads-TS denotes the adsorption of the reactant and transition state, respectively.

3. RESULTS

Because surface explosions are only observed experimentally on oxygen precovered Rh surfaces, we start with the adsorption of isolated acetate on oxygen precovered Rh. The Rh(110) and Rh(111) surfaces in our calculations contain eight and four surface Rh, respectively, and one acetate molecule occupies two adjacent surface Rh sites. Therefore, the coverage for our calculations describing the decomposition of isolated acetate on Rh(110) and Rh(111) is 0.25 and 0.50 ML, respectively.

3.1. Adsorption of Acetate. For acetate adsorption, we considered three adsorption geometries: bidentate bridging (BB) with two oxygen atoms of acetate binding to two adjacent surface metal atoms, bidentate chelating (B) with two oxygen atoms of acetate binding to one surface metal atom, and a monodentate (M) configuration with one oxygen binding to one surface metal atom. For BB configurations, we separately considered molecules bonded to Rh1−Rh2 and Rh1−Rh3 on O−Rh(110) (see Figure 1a) and Rh1−Rh2, Rh1−Rh3, Rh1−Rh4, and Rh2−Rh4 on O−Rh(111) (see Figure 1b). For each case, we considered initial geometries with various tilt angles with respect to the surface normal. Our results show that the BB structure is the most stable, which is not consistent with a previous experimental proposal.[26] Experimentally, Li et al.

dx.doi.org/10.1021/cs400826d | ACS Catal. 2014, 4, 944−953

proposed that the B configuration is the most stable based on an analogy with Cu(110).[26] However, our results show that the B structure is 0.38 and 2.38 eV less favorable than BB structure on O−Rh(110) and O−Rh(111), respectively. All attempts to obtain the M structure on O−Rh(110) resulted in the BB structure. On O−Rh(111), the M configuration was found to be a local minimum in energy that is 0.23 eV less stable than the BB structure. On O−Rh(111), the stability of acetate adsorption follows the sequence BB > M > B.

3.2. Decomposition of Isolated Acetate on Oxygen Precovered Rh Surface. Although the surface explosion only happens when a dense layer of acetate exists, we began our investigation of the acetate decomposition pathway by examining isolated acetate molecules.

3.2.1. Acetate Decomposition on Oxygen Precovered Rh(110). We studied the decomposition of acetate step by step. For each step, we considered two competing reaction paths: dehydrogenation and C−C bond cleavage. In the first step, the dehydrogenation of acetate to yield CH_2COO is less favorable kinetically and thermodynamically than C−C bond cleavage. C−C bond cleavage to yield CH_3 and CO_2 occurs with a barrier of 1.66 eV with an imaginary frequency of 288 cm^{-1} and reaction energy of −0.40 eV. The barrier for the dehydrogenation is 2.56 eV with an imaginary frequency of 716 cm^{-1}, and the reaction is endothermic by 0.58 eV. We therefore only considered products that can form following C−C bond cleavage, as shown in Figure 2. The dehydrogenation of CH_3 to

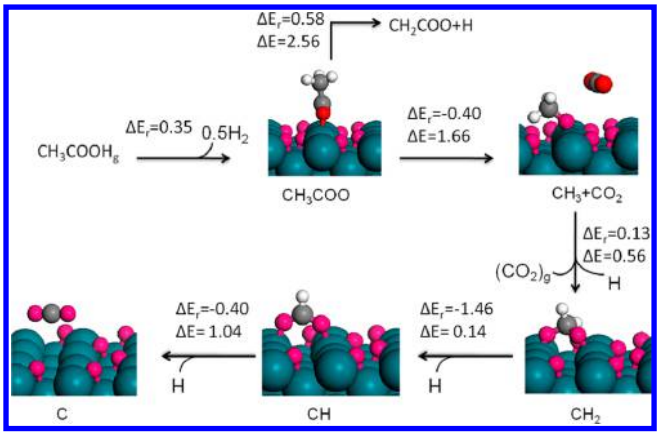

Figure 2. Reaction mechanism of decomposition of acetic acid on O−Rh(110). The reaction energy ΔE_r and reaction barrier ΔE are labeled in eV. Species in the gas phase are labeled by a subscript g. Blue large spheres: Rh; red spheres: O; pink spheres: precovered O; gray spheres: C; white spheres: H. The labels below each frame indicate the atoms from the original acetic acid visible in the frame.

yield CH_2 has a barrier of 0.56 eV, and the reaction is endothermic by 0.13 eV. The first and second dehydrogenation of CH_2, to leave C on the surface, occurs with barriers of 0.14 and 1.04 eV, respectively. Both reactions are exothermic with reaction energies of −1.46 and −0.40 eV, respectively. The H atom from dehydrogenation of CH_3 prefers to adsorb on the precovered oxygen site to form OH; further reaction with H to release H_2O is slightly endothermic with a reaction energy of 0.16 eV (see Figure S1a in the Supporting Information). The overall reaction path, $CH_3COO \rightarrow CH_3 \rightarrow CH_2 \rightarrow CH \rightarrow C$, is summarized in Figure 2. The TS structures for the rate-limiting step is provided in section 4.1 for discussion, and the other TS structures are provided in Figure S2 in Supporting Information. The rate-limiting step is the C−C bond cleavage of acetate to yield CH_3 and CO_2. As shown in Figure 2, the reaction of CH in the last step leads to the formation of CO_2 with the O atoms in this molecule coming from the O adlayer. This outcome could be verified experimentally if isotopically labeled O atoms were used in either the adsorbed acetate or the precovered O adlayer.

3.2.2. Acetate Decomposition on Oxygen Precovered Rh(111). As with the results above for Rh(110), we began on O-covered Rh(111) by considering the decomposition pathways available for an isolated acetate molecule. Our calculations showed that acetate prefers C−C bond cleavage over dehydrogenation; C−C bond cleavage to yield CH_3 and CO_2 has a barrier of 1.34 eV with reaction energy of 0.18 eV, whereas the barrier for dehydrogenation is 1.94 eV and the reaction energy is 0.34 eV. The corresponding imaginary frequencies for C−C bond cleavage and dehydrogenation are 301 and 286 cm^{-1}. We therefore only considered products that can form following C−C bond cleavage. The dehydrogenation of CH_3 to yield CH_2 has a barrier of just 0.10 eV, and the reaction is nearly energetically neutral, with a reaction energy of −0.01 eV. The two-step dehydrogenation of CH_2 has barriers of 0.40 and 0.90 eV. The dehydrogenation of CH_2 (CH) is exothermic (endothermic) with reaction energy of −1.44 (+0.74) eV. As above, the H atom from dehydrogenation of CH_3 prefers to adsorb on the precovered oxygen site to form OH, and release of H_2O is slightly endothermic with a reaction energy of 0.24 eV (see Figure S1b in the Supporting Information). The overall reaction, $CH_3COO \rightarrow CH_3 \rightarrow CH_2 \rightarrow CH \rightarrow C$, is similar to the result on O−Rh(110) and is illustrated in Figure 3. The rate-limiting step is the C−C bond

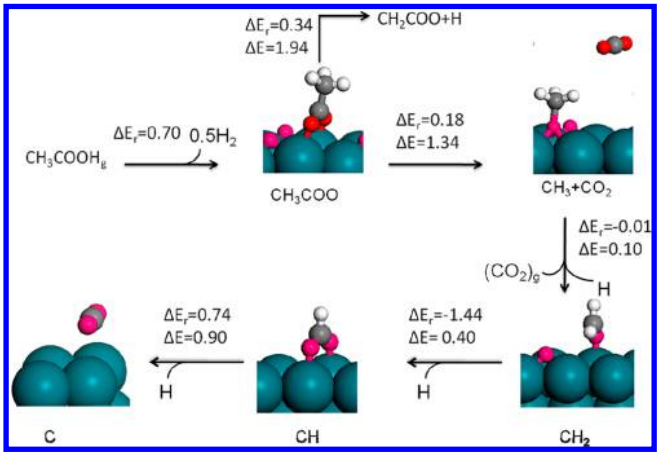

Figure 3. Reaction mechanism of decomposition of acetic acid on O−Rh(111). The reaction energy ΔE_r and reaction barrier ΔE are labeled in eV. Gas phase species are labeled by a subscript g. Blue large spheres: Rh; red spheres: O; pink spheres: precovered O; gray spheres: C; white spheres: H. The labels below each frame indicate the atoms from the original acetic acid visible in the frame.

cleavage of acetate to yield CH_3 and CO_2. The TS structure for the rate-limiting step is provided in section 4.1 for discussion, and the other TS structures are provided in Figure S3 in Supporting Information.

3.3. Acetate Decomposition from Dense Acetate Adlayers. It is clear from the experiments in which surface explosions have been observed during decomposition of acetate on O-covered Rh surfaces that this phenomenon only occurs when the surface is initially covered with a dense acetate

dx.doi.org/10.1021/cs400826d | ACS Catal. 2014, 4, 944−953

adlayer.[16,26] We therefore extended the calculations described above to consider how the reaction mechanisms that allow decomposition of acetate differ between dense adlayers and isolated adsorbed molecules.

3.3.1. Dense Acetate Adlayers on Rh(110). For dense adlayers of acetate on O−Rh(110), we considered a variety of scenarios to determine the favored adsorption configuration. We examined two initial structures in which all acetate packs along the [100] direction, as shown in Figure 4, four distinct

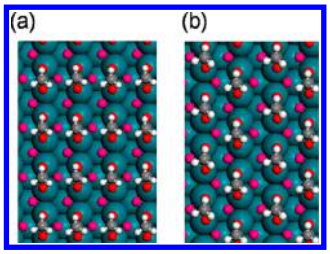

Figure 4. Dense layer for acetate adsorption on the O−Rh(110) surface: (a) parallel structure; (b) zigzag structure. Blue large spheres: Rh; red spheres: O; pink spheres: precovered O; gray spheres: C; white spheres: H.

initial structures in which all acetate packs along the [010] direction, and six additional structures that had a combination of acetate molecules oriented along the two directions. On the basis of the proposal of oxygen-induced ordering on clean Pd(110), where a surface explosion is also observed,[20] Li et al. proposed that acetate forms the parallel structure shown in Figure 4a.[16] Our calculations, however, predict that the zigzag structure shown in Figure 4b is more stable by 0.11 eV/molecule. The adsorption energy of the zigzag structure is −2.04 eV/molecule. All the other structures and their corresponding adsorption energies are shown in Figure S4 in the Supporting Information.

After identifying the geometry of the dense acetate layer, we then investigated the reaction path for dissociation of acetate in this dense layer. To initiate the reaction, an acetate in the dense layer dissociates to CH_3 and CO_2. This process has a barrier of 1.68 eV, which is very similar to the low coverage result of 1.66 eV. A transition state search showed that the favorable reaction path is the same as the single acetate on O−Rh(110), and the limiting step is still the initial C−C bond cleavage step. After this initial C−C bond cleavage, the reaction energy and barriers of the following steps are different from the case of an isolated adsorbate. In the dense adlayer, the dehydrogenation of CH_3 crosses barriers of 0.21, 1.24, and 0.69 eV. The corresponding barriers for the low coverage case, for comparison, are 0.56, 0.14, and 1.04 eV. In the final step of this process, the remaining C reacts with two surface oxygen atoms to release CO_2 into the gas phase, just like the reaction at low coverage. The hydrogen atoms from the dehydrogenation of CH_3 species can also remove one surface oxygen atom to release H_2O into the gas phase, as discussed in section 3.2. This overall reaction is summarized in Figure 5 where the reacting species are labeled by yellow ovals. All the TS structures and corresponding imaginary frequencies are shown in Figure S5 in the Supporting Information.

3.3.2. Decomposition of Isolated Acetate on Clean Rh(110). A key outcome of the reaction just described is the creation of a small clean Rh(110) area on the O−Rh(110) surface. Because subsequent reaction of nearby acetate species

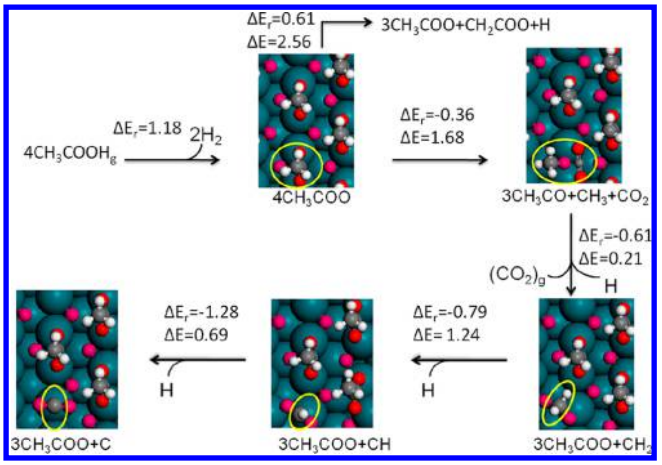

Figure 5. Reaction mechanism of decomposition of acetic acid on O−Rh(110) with a dense acetate adlayer. The reaction energy ΔE_r and reaction barrier ΔE are labeled in eV. The reacting species are labeled by the yellow ovals. Species in the gas phase are labeled by a subscript g. Blue large spheres: Rh; red spheres: O; pink spheres: precovered O; gray spheres: C; white spheres: H.

will be different from the oxygen precovered surface, we investigated the decomposition of an isolated acetate molecule on clean Rh(110). As on the oxygen precovered surface, we first identified the geometry of acetate. More information on these calculations is given in the Supporting Information. The decomposition pathway for acetate on clean Rh(110) is summarized in Figure 6. All the other TSs and corresponding

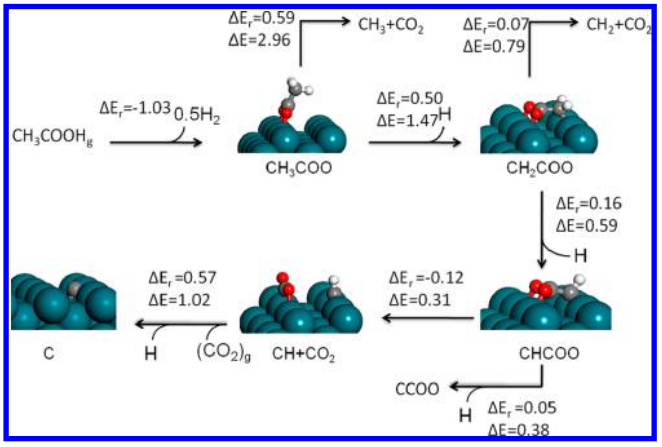

Figure 6. Reaction mechanism of decomposition of acetic acid on clean Rh(110). The reaction energy ΔE_r and reaction barrier ΔE are labeled in eV. Gas phase species are labeled by a subscript g. Blue large spheres: Rh; red spheres: O; pink spheres: precovered O; gray spheres: C; white spheres: H.

imaginary frequencies are shown in Figure S6 in the Supporting Information. There are two competitive reaction paths, C−C bond cleavage and dehydrogenation. Unlike the outcome on the oxygen precovered surface, the dehydrogenation of acetate to yield CH_2COO is favored over C−C cleavage. Dehydrogenation has a barrier of 1.47 eV with a reaction energy of 0.50 eV, although C−C cleavage has a barrier of 2.96 eV with reaction energy of 0.59 eV. The imaginary frequencies for C−C bond cleavage and dehydrogenation are 617 and 1086 cm^{-1}, respectively.

dx.doi.org/10.1021/cs400826d | ACS Catal. 2014, 4, 944−953

The further dehydrogenation of CH_2COO to yield CHCOO has a barrier of 0.59 eV, whereas the barrier for C−C bond cleavage of CH_2COO is 0.79 eV. Thus, dehydrogenation is again more favorable than C−C bond cleavage. CHCOO prefers C−C bond cleavage to form CH and CO_2 (a barrier of 0.31 eV and a reaction energy of −0.12 eV) over dehydrogenation to yield CHCOO (a barrier of 0.38 eV and a reaction energy of 0.05 eV), although both of these processes may occur in tandem. The dehydrogenation of CH to leave C on the surface presents a barrier of 1.02 eV. This reaction is endothermic with a reaction energy of 0.57 eV.

The most favorable reaction path, $CH_3COO \rightarrow CH_2COO \rightarrow CHCOO \rightarrow CH \rightarrow C$, is illustrated in Figure 6. A key observation is that this mechanism is different from the decomposition on an oxygen precovered surface. The rate-limiting step on the clean surface is the dehydrogenation of acetate to yield CH_2COO, with a calculated barrier of 1.47 eV. The energy of reaction paths including dehydrogenation and C−C bond cleavage for both pure and oxygen precovered Rh(110) surface is summarized in Figure 7. From Figure 7, we can see that the reaction path with C−C bond cleavage through CHCOO on the pure surface is most favorable among all the considered reaction paths.

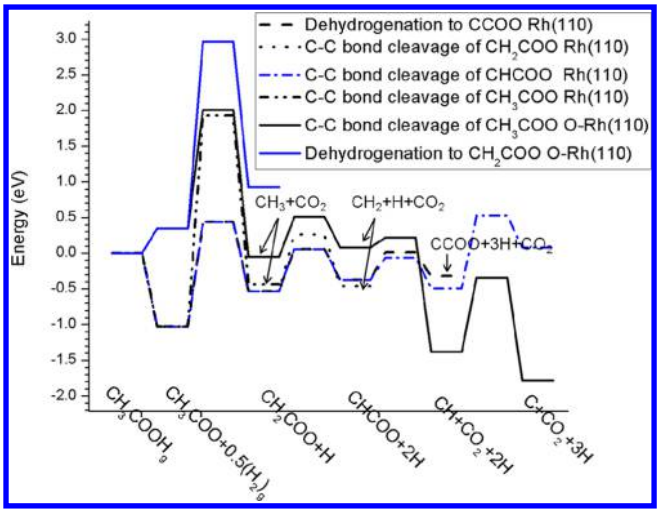

Figure 7. Energy plot of reaction path of isolated acetic acid on Rh(110) and O−Rh(110). Reaction path on O−Rh(110) is labeled by solid line. The reaction intermediates are labeled on the *x*-axis. If different from the label of the *x*-axis, the reaction intermediates are labeled in the figure. The lines between reaction intermediates are the energy of TS, which is not labeled in the figure.

We also investigated decomposition of acetate at higher but not saturated acetate coverages. The results show that the reaction at coverages of 0.50 and 0.75 ML is essentially unchanged from the outcome for an isolated acetate adsorbate (0.25 ML). For the rate-limiting step in the reaction described above, the barrier was calculated to be 1.47, 1.45, and 1.47 eV at 0.25, 0.5, and 0.75 ML initial coverage, respectively. This is consistent with the observation that the interaction energy between acetate molecules is weak in these configurations. The adsorption energy obtained from our calculations at 0.25, 0.5, and 0.75 ML was −3.36, −3.32, and −3.32 eV/molecule, respectively.

The results above suggest that the surface explosion on O−Rh(110) occurs following the mechanism illustrated in Figure 8. First, some initial acetate molecules, shown by the white bars

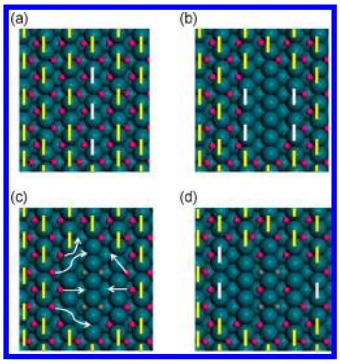

Figure 8. Schematic illustration of surface explosion on O−Rh(110) surface: (a) a dense acetate adlayer; (b) surface with a small clear region resulting from the reaction in (a); (c) surface oxygen diffusion; and (d) the small clear region shifts due to the oxygen diffusion in (c). Bars: acetate; white bars: reacting acetate in this step; blue large spheres: Rh; pink spheres: precovered O; gray spheres: C.

in Figure 8a, follow the reaction path $CH_3COO \rightarrow CH_3 \rightarrow CH_2 \rightarrow CH \rightarrow C$ with a barrier of 1.68 eV in the rate-limiting step. With the locally decreased coverage of acetate and surface oxygen, the acetate adjacent to the small clean area (white bars in Figure 8b) can react following a different reaction path that prefers dehydrogenation to form CH_2COO instead of the C−C bond cleavage. This reaction path has a rate-limiting barrier of 1.47 eV, which is 0.21 eV lower than the C−C bond cleavage of the initial acetate. Our calculations show that the barrier for diffusion of surface O is only 0.50 eV. This implies that after all the acetate near the bare surface has reacted, surface oxygen can easily diffuse from the O-covered region to the bare region, as shown in Figure 8c. As a result of surface O diffusion, the neighboring acetate, as shown by the white bar in Figure 8d, will follow the reaction path of the bare surface. We also found that it is energetically favored for acetate to move from the O-covered region to the clean region. Both this and the surface diffusion of O provide routes for moving acetate from the O-covered portions of the surface to areas of the surface that have been cleaned of oxygen by initial stages of the surface explosion.

3.3.2. Dense Acetate Adlayers on Rh(111). For the Rh(111) surface, we have performed similar calculation as on Rh(110). We first identified the configuration of a dense acetate layer and then studied the reaction path at the dense layer to explain the surface explosion. Because our unit cell has four surface Rh atoms, two adsorbed acetates in our computational volume form a dense layer. Multiple scenarios have been considered to identify the most favorable structure: (i) both acetates have a BB structure, (ii) one acetate adsorbate has a BB structure and the other acetate has a B or M structure, (iii) both acetates have a B structure, and (iv) both acetates have an M structure. For each scenario, three different initial structures with different orientations are considered. The most stable dense structure, with a combination of BB and M structures with adsorption energy of −0.95 eV/molecule, is shown in Figure 9. All the other obtained dense patterns and corresponding adsorption energies are shown in Figure S7 in the Supporting Information. We are not aware of an experimental determination of the dense layer structure on this surface.

As on O−Rh(110), we found the first acetate to decompose following the reaction path of an isolated molecules on the oxygen precovered surface, $CH_3COO \rightarrow CH_3 \rightarrow CH_2 \rightarrow CH \rightarrow C$, as shown in Figure 10, with the reacting species labeled by yellow ovals. All the TS structures and corresponding

dx.doi.org/10.1021/cs400826d | ACS Catal. 2014, 4, 944−953

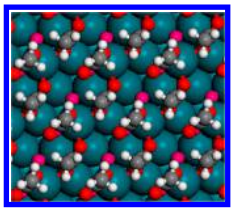

Figure 9. Dense layer for acetate adsorption on the O−Rh(111) surface. Blue large spheres: Rh; red spheres: O; pink spheres: precovered O; gray spheres: C; white spheres: H.

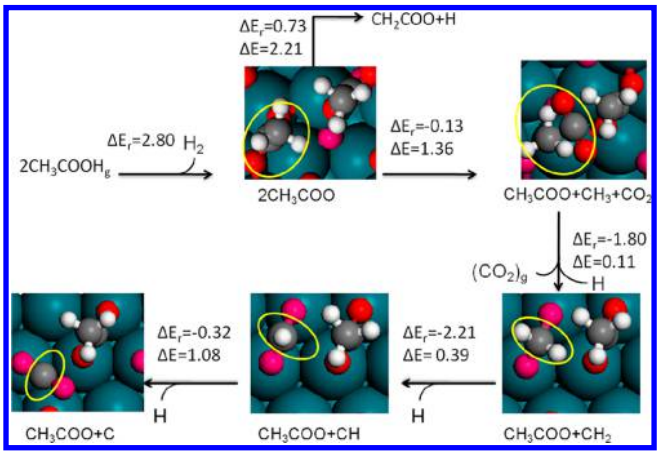

Figure 10. Reaction mechanism of decomposition of acetic acid on O−Rh(111) with a dense acetate adlayer. The reaction energy ΔE_r and reaction barrier ΔE are labeled in eV. The reacting species are labeled by the yellow oval. Species in the gas phase are labeled by a subscript g. Blue large spheres: Rh; red spheres: O; pink spheres: precovered O; gray spheres: C; white spheres: H.

imaginary frequencies are shown in Figure S8 in the Supporting Information. The rate-limiting step is still C−C bond cleavage of CH_3COO, with a barrier of 1.36 eV. The dehydrogenation of CH_3 that follows is different from the low coverage situation. The three dehydrogenation reaction energies are −1.80, −2.21, and −0.32 eV at the high coverage, although at low coverage, they are −0.01, −1.44, and 0.74 eV, respectively. The barriers for the subsequent dehydrogenation of CH_3 are close for high and low coverage. They are −0.11, 0.39, and 1.08 eV at high coverage, whereas the corresponding barriers for the low coverage are 0.10, 0.40, and 0.90 eV, respectively. Similar to the situation described above for Rh(110), the remaining C will react to remove some surface oxygen, creating a small clean Rh(111) area.

We expected the reaction path on this clear region to be different from the O-covered region of the surface, similar to what we found for Rh(110). Therefore, we studied the decomposition of acetate on a clean surface. Our results are summarized in Figure 11. The favorable reaction path changes to $CH_3COO \rightarrow CH_2COO \rightarrow CH_2 \rightarrow CH \rightarrow C$ with the barrier for the rate-limiting step at 1.19 eV. All TS structures and corresponding imaginary frequencies are shown in Figure S9 in the Supporting Information. The energy of reaction paths including dehydrogenation and C−C bond cleavage for both pure and oxygen precovered Rh(111) surface is shown in Figure 12. From Figure 12, we can see that the reaction path with C−C bond cleavage through CH_2COO on a pure surface is most favorable among all the considered reaction paths.

As on Rh(110), some initial acetates will follow the reaction path of the oxygen precovered surface and will create a small

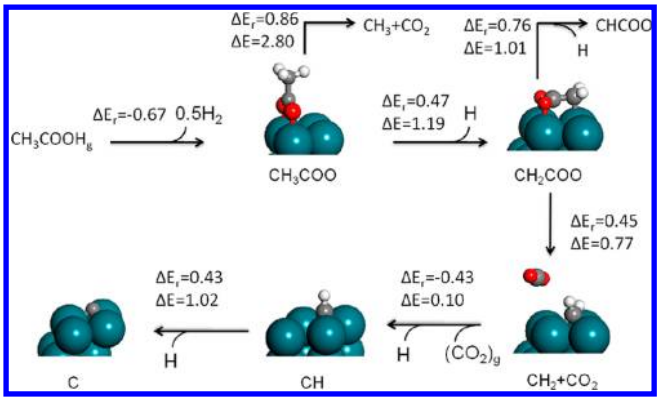

Figure 11. Reaction mechanism of decomposition of acetic acid on clean Rh(111). The reaction energy ΔE_r and reaction barrier ΔE are labeled in eV. The species in the gas phase is labeled by subscript of g. Blue large spheres: Rh; red spheres: O; pink spheres: precovered O; gray spheres: C; white spheres: H.

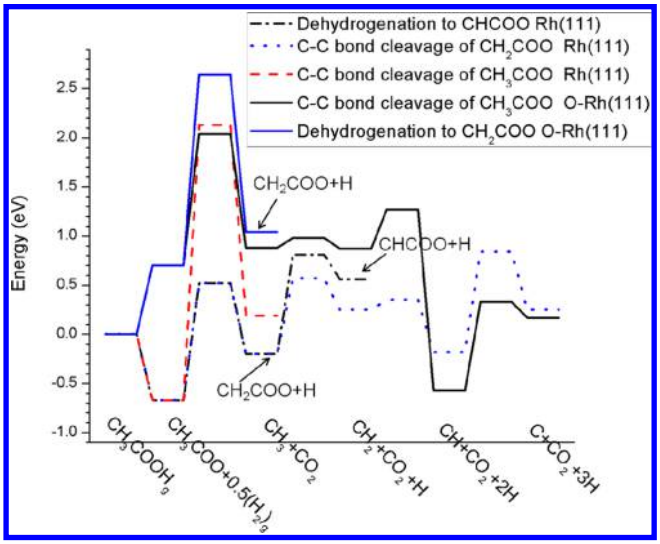

Figure 12. Energy plot of reaction path of isolated acetic acid on Rh(111) and O−Rh(111). Reaction path on O−Rh(111) is labeled by a solid line. The reaction intermediates are labeled on the *x*-axis. If different from the label of the *x*-axis, the reaction intermediates are labeled in the figure. The lines between reaction intermediates are the energy of TS, which is not labeled in the figure.

bare surface region in the end of reaction. The acetate in the bare surface region can then react by a different mechanism. Following that, surface oxygen will diffuse from the oxygen covered surface to the clear region. The diffusion barrier for atomic oxygen diffusion on the Rh(111) surface is around 0.50 eV.[41,42] This suggests that the remaining acetate molecules are able to follow the reaction path associated with the bare surface.

4. DISCUSSION

4.1. Comparison of Rate-Limiting Steps on the Clean and Oxygen Precovered Rh Surface. As shown in Figure 13 and Figure S10, the transition states for C−C bond cleavage of acetate are quite similar on the clean and oxygen precovered Rh surface. The barrier for the oxygen precovered surface, however, is considerably lower than the clean surface, resulting in the reaction path's preference for the oxygen precovered surface. We can use $\Delta(\Delta E)$ in eq 3 to indicate what induced the switch of reaction path. Equation 3 includes two parts, the

dx.doi.org/10.1021/cs400826d | ACS Catal. 2014, 4, 944−953

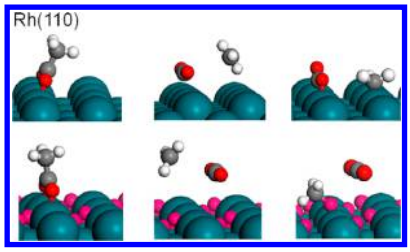

Figure 13. TS for C−C bond cleavage of acetate on clean (top) and oxygen precovered (bottom) surface. Left: reactant; middle: TS; right: product. Blue large spheres: Rh; red spheres: O; pink spheres: precovered O; gray spheres: C; white spheres: H.

difference in adsorption energy E_{ads} of reactant $[E_{ads\text{-}reactant} - E_{ads\text{-}reactant}\ (O)]$ and transition state $[E_{ads\text{-}TS}(O) - E_{ads\text{-}TS}]$.

For the decomposition of acetate on Rh(110), $[E_{ads\text{-}reactant} - E_{ads\text{-}reactant}\ (O)]$ is −1.37 eV for both dehydrogenation and C−C bond cleavage, $[E_{ads\text{-}TS}(O) - E_{ads\text{-}TS}]$ for C−C bond cleavage amounts to 0.07 eV, and $[E_{ads\text{-}TS}(O) - E_{ads\text{-}TS}]$ for dehydrogenation amounts to 2.51 eV. That is, the lower barrier for C−C bond cleavage on O−Rh(110) compared with the clean Rh(110) surface is primarily due to the reduced stability of acetate. For the dehydrogenation, E_{ads} of the reactant increased by 1.37 eV, and E_{ads} of the TS increased by 2.51 eV, resulting in the barrier for dehydrogenation increased by 1.14 eV on O−Rh(110) compared to clean Rh(110). Therefore, the change of barrier in dehydrogenation is not only due to the reduced stability of acetate reactant but also to the reduced stability of the TS.

A similar result is found on O−Rh(111) and Rh(111). The barrier for C−C bond cleavage on O−Rh(111) decreased by 1.46 eV compared with the clean Rh(111) surface, with the reduced stability of acetate contributing 1.34 eV and the increased stability of TS only contributing 0.12 eV. The change in the barrier for dehydrogenation is not only due to the reduced stability of acetate reactant, which contributes 1.34 eV, but also to the reduced stability of the TS, which contributes 2.23 eV.

4.2. Comparison of Surface Reactivity. The energy barriers listed in Table 1 indicate that Rh(111) is more active than Rh(110) for both clean and oxygen precovered surfaces. This is consistent with experimental results.[16,18] The barriers also imply that the oxygen precovered surfaces are less active than the clean surface, which is also consistent with experimental results.[16,18] In ref 18, the reaction rate reached its maximum at time t = 25.2 and 32 s with the TPD starting at 300 K on clean Rh(111) and O−Rh(111) surface, respectively. In ref 16, the reaction rate reached its maximum at time t = 51 and 110 s with the TPD starting at 315 K on clean Rh(110) and O−Rh(110) surface, respectively.

Table 1. Reaction Barrier ΔE (eV) of the Rate-Limiting Step for Different Rh Surfaces

surface	ΔE
Rh(110)	1.47
O−Rh(110)	1.66
Rh(111)	1.19
O−Rh(111)	1.34

4.3. Role of Precovered Oxygen. It is clear from experimental studies that precovering the surface with oxygen is critical to observing a surface explosion. As discussed in section 1, several possible origins of this effect from surface oxygen have been suggested:[16,17] (1) oxygen-induced surface reconstruction, (2) oxygen-induced adsorbate ordering leading to inhibition of reactivity, and (3) site blocking by surface oxygen. Our results indicate that the third of these effects is sufficient to explain the observed experimental behavior. In this role, the oxygen acts as a poison that blocks the sites adjacent to adsorbed acetate that are necessary for decomposition. The dehydrogenation of acetate on a clean surface yields the flat CH_2COO species, which adsorbs on the surface Rh sites. On an oxygen precovered Rh(110) surface, the surface oxygen blocks the adsorption with surface Rh sites, and CH_2COO ends up binding with this surface oxygen instead of the surface Rh sites (see Figure S11 in the Supporting Information). The change in binding site creates a higher reaction barrier than exists on the clean surface, preventing further dehydrogenation of acetate. Thus, C−C bond cleavage becomes more favorable. Unlike the low oxygen coverage where oxygen is found to facilitate acetate decomposition,[24] our studies show saturated oxygen coverage hinders acetate decomposition. We also found that the presence of oxygen affects the adsorption configurations (see Supporting Information). To help understand the effect of oxygen on adsorption of dense acetate adlayers, we also examined dense adlayers on clean Rh(111). For adsorption of two acetates on a clean Rh (111) surface to form a dense acetate adlayer, all attempts to obtain structures with two M adsorbates or structures with one BB molecule and one M molecule resulted in two BB adsorbates. On the oxygen precovered surface, this scenario is reversed, and structures with two BB adsorbates are unstable.

4.4. Simulation of Temperature Programmed Desorption. In our previous discussion, we proposed a heuristic model to explain the surface explosion observed for acetate on Rh surfaces. In order to make a more direct comparison with experiments, we performed simulations of TPD using a model motivated by the DFT calculations described above. In this model, we assume a single step reaction controlled by the rate-limiting step in the more complex multistep reaction characterized by our DFT calculations. Below, we first describe a TPD simulation for the decomposition of isolated acetate molecules, corresponding to low acetate coverage. We then extend this simulation to adlayers that are initially saturated on the surface.

4.4.1. TPD Simulation for Isolated Acetate Species. For a clean surface, the rate-limiting step is the dehydrogenation of acetate, $CH_3COO^* + {}^* \rightarrow CH_2COO^* + H^*$. Our kinetic model is a simplified description that only considers this rate-limiting step. The dehydrogenation of acetate requires an extra vacant site to allow formation of the flat CH_2COO species. Therefore r is not only a function of acetate coverage, θ_{CH_3COO}, but also of vacant sites, $(1 - \theta_{CH_3COO})$:

$$r = -\frac{d\theta_{CH_3COO}}{dt} = A\exp\left[\frac{-\Delta E}{R(T_0 + \beta t)}\right]\theta_{CH_3COO}(1 - \theta_{CH_3COO}) \quad (4)$$

where T_0 is the initial temperature for a TPD experiment, and β is the heating rate. For an oxygen precovered surface, the rate-limiting step is the C−C bond cleavage of acetate, $CH_3COO^* \rightarrow CH_3^* + (CO_2)_g$. C−C bond cleavage does not require an extra vacant site, because it releases CO_2 into the gas phase in the rate-limiting step. Therefore, r is only a function of acetate coverage, θ_{CH_3COO}:

dx.doi.org/10.1021/cs400826d | ACS Catal. 2014, 4, 944−953

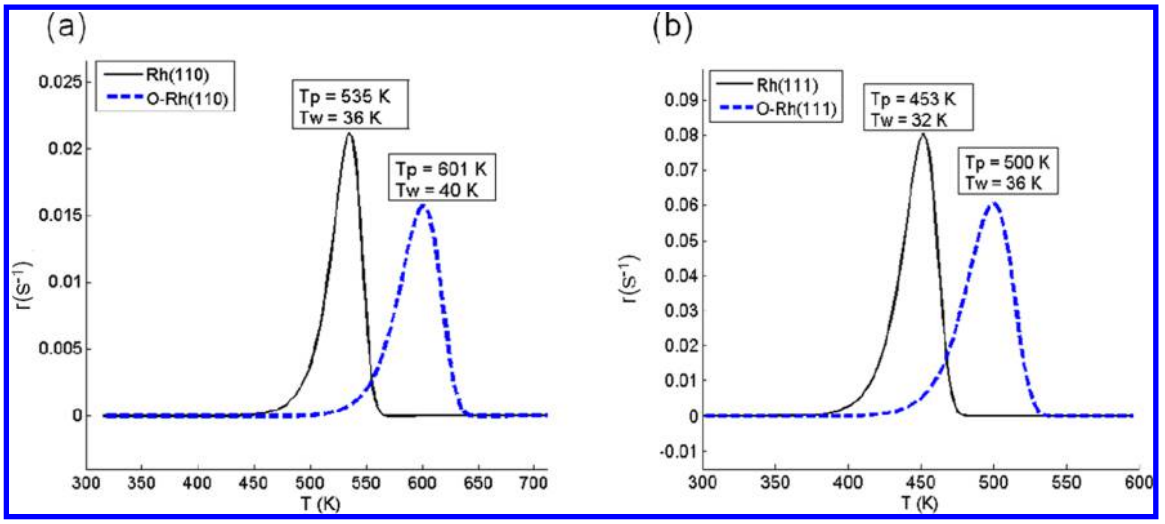

Figure 14. Simulation of TPD on clean (black curves) and oxygen precovered (blue dashed curves) surface for acetate with a low initial coverage. (a) Rh(110) with T_0 = 315 K and β = 1.5 K/s. (b) Rh(111) with T_0 = 300 K and β = 5 K/s. The peak temperature, T_p, and full width at half-maximum, T_w, is shown for each simulation.

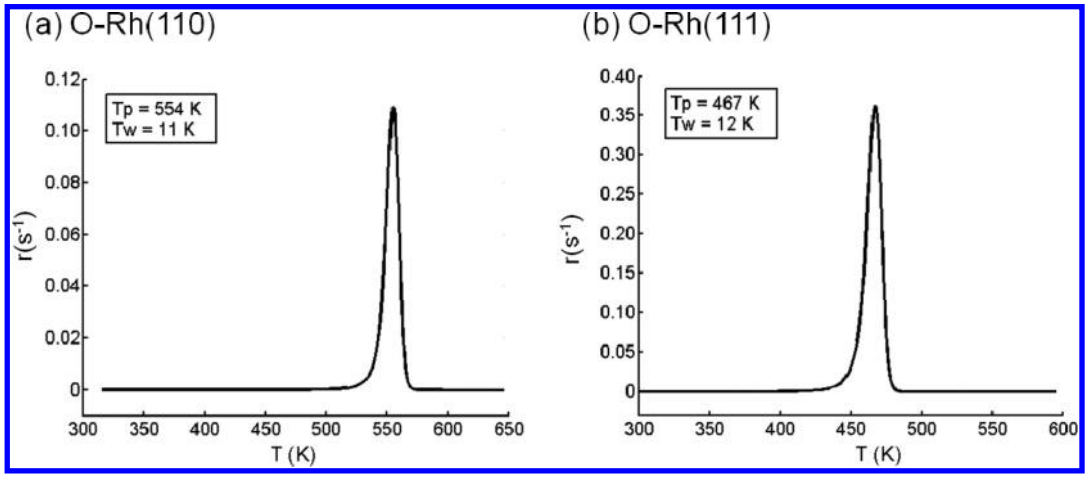

Figure 15. Simulation of TPD on oxygen precovered Rh surface for dense layer with a saturated initial coverage. (a) O−Rh(110) with T_0 = 315 K and β = 1.5 K/s. (b) O−Rh(111) with T_0 = 300 K, and β = 5 K/s. The peak temperature, T_p, and full width at half-maximum, T_w, is shown for each simulation.

$$r = -\frac{d\theta_{CH_3COO}}{dt} = A\exp\left[\frac{-\Delta E}{R(T_0 + \beta t)}\right]\theta_{CH_3COO} \quad (5)$$

In eqs 4 and 5, A was set to 10^{13} s^{-1}.[43] The initial temperature T_0 and heating rate were taken from experiments:[16,18] for Rh(110), T_0 was 315 K and β = 1.5 K/s, whereas for Rh(111), T_0 was 300 K, and β = 5 K/s. Reaction barriers, ΔE, were taken from our DFT calculation: 1.47 (1.66 eV) for clean (oxygen covered) Rh(110) and 1.19 (1.34) eV for clean (oxygen covered) Rh(111). To mimic low initial coverages, the initial value of θ_{CH_3COO} was set to be 0.25 and 0.5 for Rh(110) and Rh(111) surface, respectively. The reaction rate is integrated by the ordinary differential equation solver (ode23) on the basis of the second/third-order Runge−Kutta method in MATLAB 7.[44]

The results of our simulations for low initial acetate coverages are shown in Figure 14. The peak temperature, T_p, on the oxygen precovered surface is considerably higher than on the clean surface. No surface explosion is observed with low initial coverage of acetate. In our simulations, $T_w \sim 40$ K, consistent with experimental results.[18] Hoogers et al.[18] found that with a low acetate coverage on the clean Rh(111) surface, TPD yields a desorption peak temperature of T_p = 411 K, and T_w = 34 K.

4.4.2. TPD Simulation for Surface Explosion. As we proposed in Sec. 3.3, during the surface explosion, some initial acetates followed the reaction path on the oxygen precovered surface, where the rate-limiting step is $CH_3COO^* \xrightarrow{K_u} CH_3^* + (CO_2)_g$ In this trigger reaction, the C−C bond cleavage does not require an extra vacant site since it releases CO_2 into the gas phase. With the decreased coverage of acetate and surface oxygen, the remaining acetate may follow the reaction path of the decomposition of acetate on the clean surface. The corresponding rate-limiting step is $CH_3COO^* + * \xrightarrow{K_e} CH_2COO^* + H^*$. The dehydrogenation of acetate requires an extra vacant site to adopt the CH_2COO and H species in the rate-limiting step. Therefore, the reaction rate for the surface explosion will include two parts, as shown in eq 6. In eq 6, the first term corresponds to the reaction rate of the trigger reaction, and the second term corresponds to the reaction rate of dehydrogenation reaction. As above, the model

dx.doi.org/10.1021/cs400826d | ACS Catal. 2014, 4, 944−953

is a simplified model which only considers the rate-limiting step. This gives

$$r = -\frac{d\theta_{CH_3COO}}{dt} = r_4 + r_5 = k_n\theta_{CH_3COO} + k_e\theta_{CH_3COO}(1 - \theta_{CH_3COO}) \quad (6)$$

where $k_n = A_n\exp[-(\Delta E)_n/R(T_0 + \beta t)]$ and $k_e = A_e\exp[-(\Delta E)_e/R(T_0 + \beta t)]$. A_n and A_e were both chosen to be 10^{13} s^{-1}.[43] The initial temperature T_0 and heating rate is taken from experiments where for O−Rh(110), T_0 is 315 K and β= 1.5 K/s, and for O−Rh(111), T_0 is 300 K, and β = 5 K/s.[16,18] Reaction barriers were taken from our DFT calculations: $(\Delta E)_n$ is 1.68 and 1.36 eV for O−Rh(110) and O−Rh(111), respectively, and $(\Delta E)_e$ is 1.47 and 1.19 eV for O−Rh(110) and O−Rh(111), respectively. The initial value of θ_{CH_3COO} is set to be 1. At t = 0, the second term in eq 6 is zero, so only the trigger reaction plays a role in the reaction rate. As the reaction proceeds, however, both reactions contribute to the overall reaction rate.

We used eq 6 to simulate the TPD of acetate decomposition on Rh(110) and Rh(111), as shown in Figure 15. On O−Rh(110)), the resulting peak temperature is 554 K, and T_w is 11 K. The corresponding experimental value is 465 and 16 K, respectively.[16] For O−Rh(111), T_p = 467 K, and T_w = 12 K in our simulation. The corresponding experimental values are 460 and 12 K, respectively.[18] Given the simplicity of the model underlying our TPD simulation, the agreement between the experimental and simulated results is good. In principle, a more detailed model could be developed that included multiple steps of the underlying reaction or that used Monte Carlo methods to assess the potential role of spatial inhomogeneities in the reacting adlayer, but this is beyond the scope of this manuscript.

5. CONCLUSION

We have used periodic density functional theory calculations to explain the "surface explosion" observed for decomposition of acetate on oxygen precovered Rh surfaces. Our results examined Rh(110) and Rh(111), but the observation of similar phenomena on supported Rh catalysts[17] supports the concept that the same mechanism applies for more structurally complex supported metal particles. To explain the surface explosion, we first studied the decomposition of an isolated acetate and then examined the reaction of the dense layer on oxygen precovered surfaces. The rate-limiting step is C−C bond cleavage, with an energy barrier of 1.66 and 1.34 eV for an isolated acetate on O−Rh(110) and O−Rh(111), respectively. The favorable reaction path is $CH_3COO \rightarrow CH_3 \rightarrow CH_2 \rightarrow CH \rightarrow C$. A key outcome of the reaction just described is the creation of a small clean Rh surface area on the O−Rh surface. Because subsequent reaction of nearby acetate species will be different from the oxygen precovered surface, we then investigated the decomposition of an isolated acetate molecule on the clean Rh surface. On this clean Rh surface area, the remaining acetate proceeds via a dehydrogenation reaction pathway. The favorable reaction path changes to $CH_3COO \rightarrow CH_2COO \rightarrow CHCOO \rightarrow CH \rightarrow C$ on Rh(110) and $CH_3COO \rightarrow CH_2COO \rightarrow CH_2 \rightarrow CH \rightarrow C$ on Rh(111). The barrier of the rate-limiting step is around 0.20 eV smaller than the initial decomposition barrier of acetates on the O−Rh surface. Our calculations show that the barrier for diffusion of surface O is only 0.50 eV. This implies that after all the acetate near the bare surface has reacted, surface oxygen can easily diffuse from the O-covered region to the bare region. As a result of surface O diffusion, the neighboring acetate will follow the reaction path of the bare surface. We also found that it is energetically favorable for acetate to move from the O-covered region to the clean region. Both this and the surface diffusion of O provide routes for moving acetate from the O-covered portions of the surface to areas of the surface that have been cleaned of oxygen by the initial stages of the surface explosion.

We have used our DFT results to propose a simplified microkinetic model for acetate decomposition that is suitable for simulating TPD. Our TPD simulations show that no surface explosion will be observed for low initial coverages of acetate and that the desorption peak has a fwhm value of around 40 K. Under conditions leading to a surface explostion, however, our TPD simulations give a fwhm of 11 K for O−Rh(110) surface and 12 K for O−Rh(110) surface, close to the experimental value of 16 and 12 K, respectively.[16,18] The corresponding peak temperature, T_p, is 554 K on O−Rh(110) surface and 467 K for O−Rh(111) surface, which are 89 higher and 7 K higher than experimental values, respectively.

Our results provide a molecular-level explanation of the acetate surface explosion. As a site blocking agent, the precovered oxygen hinders adsorbed molecules in the close-packed layer from reacting with surface metal atoms. As a result, a surface reaction initiates when adsorbed acetate follows the reaction path available on the oxygen precovered surface, creating a small bare surface region at the end of reaction. Acetate can then react via a different mechanism in this bare region. At the same time, surface oxygen can diffuse from oxygen-covered regions of the surface to the bare regions of the surface, making it possible for further adsorbed acetate molecules to react without the site-blocking effect of oxygen. These results show that it is not necessary to invoke the existence of oxygen-induced surface reconstructions or other oxygen-induced ordering effects to understand the origin of surface explosions on these surfaces.

To the best of our knowledge, this is the first example of a surface explosion for which the underlying reaction mechanism has been understood at a molecular level. Although no generality can be claimed about the mechanism for other adsorbates and surfaces for which surface explosions can occur, our results do illustrate the possibility of combining DFT and microkinetic models to understand these fascinating reactions. The reaction mechanisms that are determined in this way will be useful for describing these systems both during variable temperature experiments of the kind usually associated with surface explosions and also under more catalytically relevant steady state conditions.

■ ASSOCIATED CONTENT

Supporting Information

Geometry of acetate on the clean Rh surface. Formation of H_2O on the oxygen precovered surface. TS for dehydrogenation of CH_3 on the oxygen precovered Rh(110) surface. TS for dehydrogenation of CH_3 on the oxygen precovered Rh(111) surface. Other adsorption patterns for dense acetate on the oxygen precovered Rh(110) surface. TS for each elementary step on oxygen precovered Rh(110) for the dense acetate adlayer. TS for each elementary step on clean Rh(110). Bond distance of the bond being broken for each elementary step on the clean Rh(110) surface. Other adsorption patterns for dense acetate on the oxygen precovered Rh(111) surface. TS for each elementary step on oxygen precovered Rh(111) for

dx.doi.org/10.1021/cs400826d | ACS Catal. 2014, 4, 944−953

the dense acetate adlayer. TS for each elementary step on clean Rh(111). Bond distance of the bond being broken for each elementary step on the clean Rh(111) surface. TS for C−C bond cleavage of acetate on the pure and oxygen precovered Rh(111) surface. TS for dehydrogenation of acetate on the clean and oxygen precovered Rh(110) surface. The role of oxygen and its effect on adsorption. This material is available free of charge via the Internet at http://pubs.acs.org.

AUTHOR INFORMATION

Corresponding Author

*E-mail: david.sholl@chbe.gatech.edu.

Notes

The authors declare no competing financial interest.

ACKNOWLEDGMENTS

This work was supported by the Department of Energy under Grant No. DE-FG02-09ER16078.

REFERENCES

(1) Cheong, W. Y.; Huang, Y.; Dangaria, N.; Gellman, A. J. *Langmuir* **2010**, *26*, 16412−16423.
(2) Hedström, M.; Cheng, H.-P. *J. Phys. Chem. B* **2000**, *104*, 4633−4641.
(3) Morgan, C.; Bowker, M. *Surf. Sci.* **2009**, *603*, 54−59.
(4) Li, Z. J.; Gao, F.; Tysoe, W. T. *Surf. Sci.* **2008**, *602*, 416−423.
(5) Romer, S.; Behzadi, B.; Fasel, R.; Ernst, K. H. *Chem.—Eur. J.* **2005**, *11*, 4149−4154.
(6) Alemozafar, A. R.; Madix, R. J. *J. Phys. Chem. B* **2004**, *108*, 14374−14383.
(7) Haley, R. D.; Tikhov, M. S.; Lambert, R. M. *Catal. Lett.* **2001**, *76*, 125−130.
(8) Li, B.; Griffiths, K.; Zhang, C. S.; Norton, P. R. *Surf. Sci.* **1997**, *384*, 70−80.
(9) Date, M.; Okuyama, H.; Takagi, N.; Nishijima, M.; Aruga, T. *Surf. Sci.* **1995**, *341*, L1096−L1100.
(10) Meng, B.; Jachimowski, T. A.; Sun, Y.; Weinberg, W. H. *Surf. Sci.* **1994**, *315*, L959−L963.
(11) Roth, C.; Ernst, K. H. *Top. Catal.* **2011**, *54*, 1378−1383.
(12) Lawton, T. J.; Pushkarev, V.; Wei, D.; Lucci, F. R.; Sholl, D. S.; Gellman, A. J.; Sykes, E. C. H. *J. Phys. Chem. C* **2013**, *117*, 22290−22297.
(13) Mhatre, B. S.; Pushkarev, V.; Holsclaw, B.; Lawton, T. J.; Sykes, E. C. H.; Gellman, A. J. *J. Phys. Chem. C* **2013**, *117*, 7577−7588.
(14) Behzadi, B.; Romer, S.; Fasel, R.; Ernst, K. H. *J. Am. Chem. Soc.* **2004**, *126*, 9176−9177.
(15) Madix, R. J.; Falconer, J. L.; Suszko, A. M. *Surf. Sci.* **1976**, *54*, 6−20.
(16) Li, Y.; Bowker, M. *J. Catal.* **1993**, *142*, 630−640.
(17) Cassidy, T. J.; Allen, M. D.; Li, Y.; Bowker, M. *Catal. Lett.* **1993**, *21*, 321−331.
(18) Hoogers, G.; Papageorgopoulos, D. C.; Ge, Q.; King, D. A. *Surf. Sci.* **1995**, *340*, 23−35.
(19) Bowker, M.; Cassidy, T. J. *J. Catal.* **1998**, *174*, 65−71.
(20) Bowker, M.; Morgan, C.; Couves, J. *Surf. Sci.* **2004**, *555*, 145−156.
(21) Aas, N.; Bowker, M. *J. Chem. Soc., Faraday Trans.* **1993**, *89*, 1249−1255.
(22) Makeev, A. G.; Nieuwenhuys, B. E. *J. Chem. Phys.* **1998**, *108*, 3740−3749.
(23) Alas, S. J.; Vicente, L. *J. Chem. Phys.* **2008**, *128*, 8.
(24) Hansen, E.; Neurock, M. *J. Phys. Chem. B* **2001**, *105*, 9218−9229.
(25) Vicente, L.; Caballero, F. V. *J. Mol. Catal. A: Chem.* **2007**, *272*, 118−127.
(26) Li, Y.; Bowker, M. *Surf. Sci.* **1993**, *285*, 219−226.
(27) Lemonidou, A. A.; Vagia, E. C.; Lercher, J. A. *ACS Catal.* **2013**, 1919−1928.
(28) Bowker, M.; Cassidy, T. J.; Allen, M. D.; Li, Y. *Surf. Sci.* **1994**, *307*, 143−146.
(29) Sholl, D. S.; Steckel, J. A. *Density functional theory: a practical introduction*; John Wiley & Sons, Inc.: Hoboken, NJ, 2009
(30) Perdew, J. P.; Chevary, J. A.; Vosko, S. H.; Jackson, K. A.; Pederson, M. R.; Singh, D. J.; Fiolhais, C. *Phys. Rev. B* **1992**, *46*, 6671−6687.
(31) Perdew, J. P.; Wang, Y. *Phys. Rev. B* **1992**, *45*, 13244−13249.
(32) Kresse, G.; Hafner, J. *Phys. Rev. B* **1993**, *47*, 558−561.
(33) Kresse, G.; Furthmüller, J. *Comput. Mater. Sci.* **1996**, *6*, 15−50.
(34) Kresse, G.; Furthmüller, J. *Phys. Rev. B* **1996**, *54*, 11169−11186.
(35) Kresse, G.; Joubert, D. *Phys. Rev. B* **1999**, *59*, 1758−1775.
(36) Henkelman, G.; Uberuaga, B. P.; Jonsson, H. *J. Chem. Phys.* **2000**, *113*, 9901−.
(37) Sheppard, D.; Terrell, R.; Henkelman, G. *J. Chem. Phys.* **2008**, *128*, 134106.
(38) Choi, Y.; Liu, P. *J. Am. Chem. Soc.* **2009**, *131*, 13054−13061.
(39) Dri, C.; Africh, C.; Esch, F.; Comelli, G.; Dubay, O.; Koehler, L.; Mittendorfer, F.; Kresse, G.; Dudin, P.; Kiskinova, M. *J. Chem. Phys.* **2006**, *125*, 094701.
(40) Ganduglia-Pirovano, M. V.; Scheffler, M. *Phys. Rev. B* **1999**, *59*, 15533−15543.
(41) Mavrikakis, M.; Rempel, J.; Greeley, J.; Hansen, L. B.; Norskov, J. K. *J. Chem. Phys.* **2002**, *117*, 6737−6744.
(42) Inderwildi, O. R.; Lebiedz, D.; Deutschmann, O.; Warnatz, J. *J. Chem. Phys.* **2005**, *122*, 034710.
(43) Sharpe, R. G.; Bowker, M. *J. Phys.: Condens. Matter* **1995**, *7*, 6379−6392.
(44) Pratap, R. *Getting Started With Matlab 7: A Quick Introduction For Scientists And Engineers*; Oxford University Press, Inc.: New York, 2006.